

Influence of the Properties of a Real Semi Anechoic Chamber on an Internal Electromagnetic Field Distribution

MARTIN POSPISILIK, JOSEF SOLDAN, MILAN ADAMEK

Faculty of Applied Informatics
Tomas Bata University in Zlin
Nad Stranemi 4511, 760 05 Zlin
CZECH REPUBLIC
pospisilik@fai.utb.cz

Abstract: - This paper describes an experiment dealing with monitoring of an electrical field displacement within a real semi anechoic chamber of an irregular shape. The experiment is based on the assumption that the semi anechoic chamber acts as a cavity resonator, and the possibilities of the internal frequency modes of damping are technically limited. In semi anechoic chambers for electromagnetic compatibility testing, this phenomenon leads to a variation of the field strength in the space of the chamber, which may affect the accuracy of the measurement. Therefore, accurate mapping of the chamber's influence to the measurement can help the engineers to improve the methods of equipment testing on electromagnetic compatibility, making it faster, more accurate and more controlled. An example of a response of the semi anechoic chamber operated at Tomas Bata University in Zlin is provided within the framework of this paper, as well as a discussion on the results obtained.

Key-Words: - Semi Anechoic Chamber, Electromagnetic Compatibility, Electrical Field Distribution, Dominant Modes

1 Introduction

Within the framework of measurements related to Electromagnetic Compatibility (EMC), measurements of Electromagnetic Interference (EMI) and Electromagnetic Susceptibility (EMS) with the aid of antennas play a dominant role. For these measurements it is necessary to ensure a low level of ambient electromagnetic interference in the range of all measured frequencies, which is almost impossible to reach without a shielded space. Unfortunately, once a shielded chamber is used for the measurements, its construction considerably affects the distribution of the electromagnetic field inside the chamber.

Both the measurement procedure and the measurement chamber construction are standardized according to international standards. The goal of the constructions is to create such internal conditions in the chamber, which correspond to measurements carried out in an open space. However, due to deviations from the ideal state, in practice the effects of the chambers to results of the measurement can be observed.

The authors of the paper are convinced that the uncertainties can be lowered by applying a correction that is based on the knowledge of the

electric and magnetic field distribution within the semi anechoic chamber.

Because at Tomas Bata University in Zlin a semi anechoic chamber is used, its behaviour was studied by mapping the electric field distribution within its space, especially at the frequencies that are expected to be close to the dominant modes of the chamber. The results of rough mapping of the spectrum inside the chamber are described in the framework of this paper.

The goal of the research consists in mapping of how the electromagnetic field inside the semi anechoic chamber is distributed and in analytical determining of corrections that could be applied to the measurement in order to improve its accuracy. According to current standards, when EMI measurements are processed, a time consuming process of moving the antenna polarization and position relative to the equipment under test must be practiced in order the maxima of interference were found. Provided the behavior of the chamber is known as well as the radiation pattern of the device, this process can be considerably shortened.

2 Problem formulation

Theoretically, the simplest measurement of Electromagnetic Interference according to the standard CISPR 16-1 can be processed at an Open Area Test Site the configuration of which is depicted in Fig. 1.

According to the standards, the measurement distance D is usually 3, 10, 30 or 100 m. The higher the distance is, the more accurate the results are, but for high distances, the level of disruptive ambient fields becomes critical [3]. The elliptical shape of the site ensures sufficient attenuation of reflected waves, provided the highly reflective surfaces are placed behind the borders of the ellipse. To ensure the reproducibility of measurements, additional specifications of the shape of the grounded metal flooring at the site are prescribed by relevant standards [3]. Then the height of the measurement antenna is adjusted in several steps and the Equipment under Test (EuT) is rotated as well in order to find the worst case of interference.

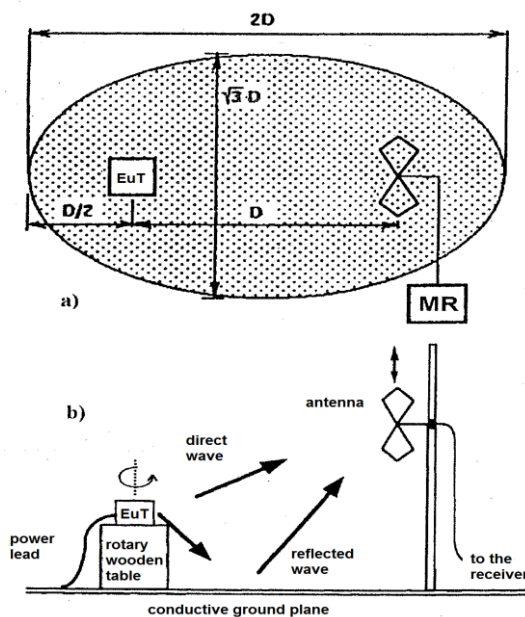


Fig. 1 Generic open area test site configuration [3]

Once the geometry of the measurement site is defined, there is a need to assure that the level of the ambient disruptive fields was at least 20 dB lower than the level of the measured interferences [3]. This condition is usually hard to achieve due to close transmitters of various radio communication channels etc. Therefore, electromagnetically shielded chambers are used to process the measurement in practice. Unfortunately, the shielded chamber acts as a cavity resonator. Its resonant frequencies can be calculated according to the following equation:

$$f_{ijk} = \frac{c}{2\pi\sqrt{\mu_r\epsilon_r}} \sqrt{\left(\frac{i\pi}{L}\right)^2 + \left(\frac{j\pi}{H}\right)^2 + \left(\frac{k\pi}{W}\right)^2} \quad (1)$$

Where:

c – field propagation velocity [m/s],

μ_r – relative permeability [-],

ϵ_r – relative permittivity [-],

i, j, k – wave indexes (case $i = j = k = 0$ is forbidden),

L – box length [m],

H – box height [m],

W – box width [m].

As a result of this, the measurement is burdened with numerous errors as there is a great variety of resonant frequencies inside the chamber. Moreover, as the walls of the chamber are reflective, multiple reflections occur as well. An illustrative frequency response of a shielded chamber without damping is depicted in Fig. 2.

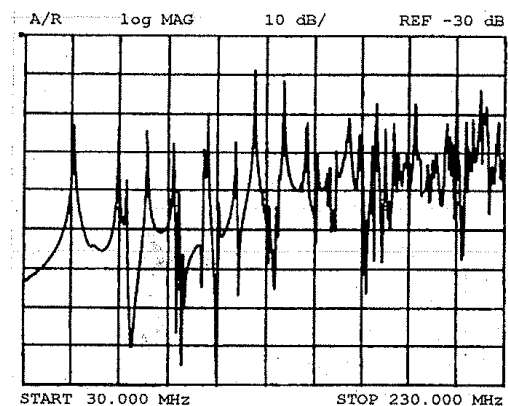


Fig. 2 Typical frequency response of undamped semi anechoic chamber [3]

It is obvious that the need for elimination of the reflections is enormous. Therefore, the inner surfaces of the shielded chamber are equipped with absorbers of different types and constructions. In this way, two types of chambers are usually constructed:

- a) A semi anechoic chamber uses absorbers on the ceiling and the walls, but there is a conductive ground plane. It acts as an Open Area Test Site. Such a chamber is suitable for measurements of EMI and EMS according to usual standards.

- b) A fully anechoic chamber uses absorbers at all surfaces. It is suitable for measuring of antenna characteristics etc.

However, in practice, the efficiency of the absorbers is limited by technical possibilities. A small amount of energy is reflected back to the space of the chamber, resulting in standing wave occurrence at various locations according to the wavelengths. The examples of reflection losses caused by absorbers are depicted in the figures below, according to their construction. In technical standards, two main approaches are defined to eliminate the phenomenon of reflections:

- The minimum efficiency of the absorbers is defined.
- The mutual position of the tested equipment and the measuring antenna is changed during the testing process.

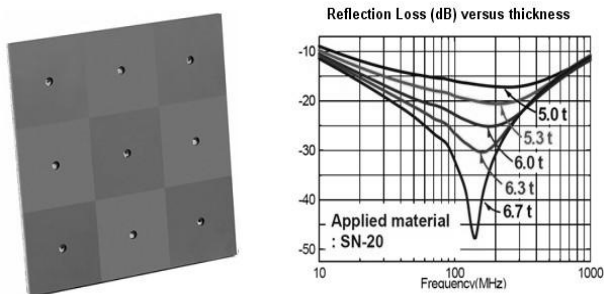


Fig. 3 Flat ferrite absorber and its performance (example) [2]

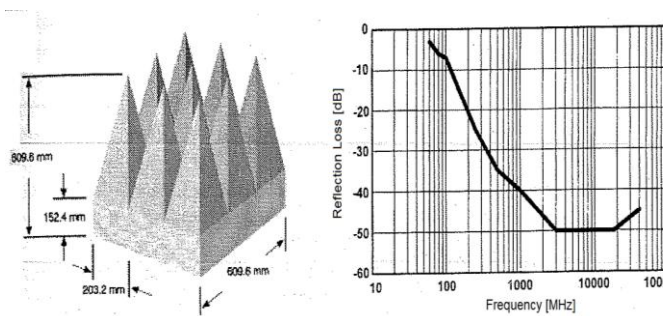


Fig. 4 Pyramidal absorbers and their performance (example) [3]

Examples on field distributions inside a resonant box are described in [1].

Usually, when the measurement is operated according to standards, measurement at different locations and mutual angles is quite time consuming. In addition, despite the above mentioned provisions, quite high uncertainty is allowed for such types of measurements. The

knowledge of the chamber’s response at different locations to various frequencies could be used to create a set of corrections that would lead to increasing the accuracy of measurements or to the acceleration of the measurements by decreasing the number of mutual positions of the equipment under test and the measuring antenna.

The experiment described in this paper was held in a semi anechoic chamber the description of which is provided below.

3 The experiment

The experiment consisted in measurement of electrical field distribution inside a semi anechoic chamber once it is driven with a rod antenna.

3.1 Description of the chamber

The experiment was held in a semi-anechoic chamber Frankonia SAC-3 plus, which is suitable for emission measurements according to EN 55022 / CISPR 22 class B and immunity tests according to IEC/EN 61000-3-4. The construction of the chamber is specific for its cylindrically shaped ceiling. The manufacturer claims that the dome shaped roof as well as its optimized absorber layout, with ferrite and partial hybrid absorber lining, minimizes the reflections in between 26 MHz and 18 GHz [4]. The frequencies used for the experiment were set close to the lower frequency limit of the chamber as it was expected to drive the first dominant mode of electrical field in this spectrum. Generic configuration of the chamber is depicted in Fig. 3.

According to the documentation, the internal dimensions of the chamber are listed in Table 1.

Table 1. Dimensions of the chamber

Length	9,680 mm
Width	6,530 mm
Height	9,500 mm (maximum)
	6,000 mm (minimum)

The height of the chamber varies according to position, as the ceiling is of cylindrical shape. The maximum height is in the longitudinal plane of the centre of the chamber, the minimum height is near the longer walls of the chamber. As the chamber is equipped with cone absorbers, the internal area is effectively restricted to approximately 8,120 x 5,150 mm.

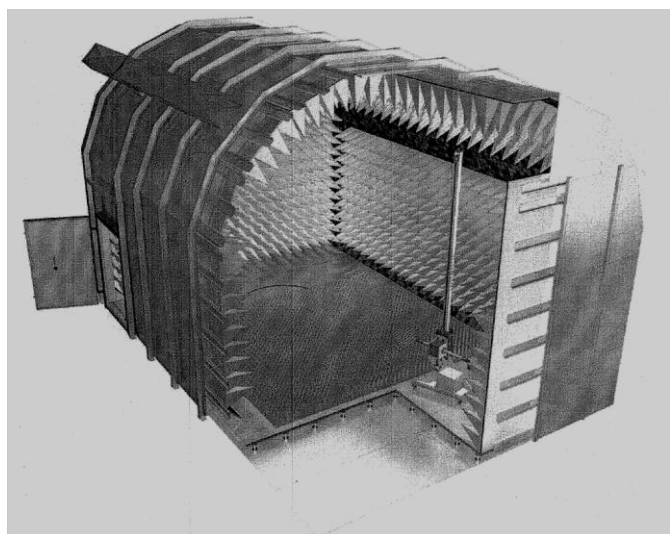


Fig. 5 Semi anechoic chamber Frankonia SAC 3 – plus [4]

3.2 Configuration of the experiment

For the purpose of the experiment, the following equipment was used:

- Semi anechoic chamber Frankonia SAC 3-plus equipped with pyramidal and flat ferrite absorbers
- Omnidirectional transmitting antenna (monopole) with a tripod
- Anisotropic spherical probe HZ-11 [5] with a tripod,
- Signal generator Rohde & Schwarz SMB 100A,
- EMI Test Receiver Rohde & Schwarz ESU,
- Controlling computer,
- Set of coaxial cables.

Displacement of the measurement points in the chamber is depicted in Fig. 6.

The measurement was realized at 15 points (A) to (O). The central point (H) was located in the middle of the chamber's floor. According to the dimensions of the chamber, the distance among the neighbouring points was 1,300 mm.

Behind the points (F) and (K) a passive semi-logarithmical antenna was left at a height of 4,000 mm. Between the points (I) and (J) there was a wooden table on which the Equipment under Test is placed where the tests are processed. Between points (H) and (I) an omnidirectional transmitting antenna (monopole) was placed (ANT). The antenna was fed with the power of 1 mW (0 dBm) in order to drive the electromagnetic field inside the

chamber. The levels of electrical fields at the points (A) to (O) were measured with Rohde & Schwarz omnidirectional spherical field probe HZ-11. The field probe was always placed at a height of 1,500 mm.

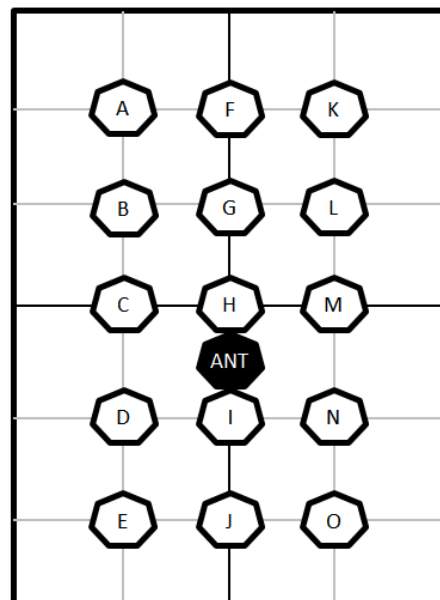


Fig. 6 Displacement of the measurement points in the chamber

3.3 Expectations

Based on the below mentioned theory, the chamber was expected to resonate at the frequencies close to 30 MHz. Because the shape of the chamber combines two model cases – a cuboid and a cylinder, three cases were theoretically analysed:

- Cuboidal resonator with the height of 6,000 mm (minimum height)
- Cuboidal resonator with the height of 9,500 mm (maximum height)
- Cylindrical resonator

According to the above mentioned cases, two dominant modes were expected: TE_{101} (for cuboidal resonator) and TE_{111} (for cylindrical resonator). Because the height of the chamber is omitted for TE_{101} , for the cases a) and b) the resonant frequency can be calculated as follows:

$$\lambda_{01}^{TE_{101}} = \lambda_{02}^{TE_{101}} = \frac{2\pi}{\sqrt{\left(\frac{i\pi}{a}\right)^2 + \left(\frac{j\pi}{b}\right)^2 + \left(\frac{k\pi}{c}\right)^2}}$$

$$= \frac{2\pi}{\sqrt{\left(\frac{1 \cdot \pi}{6.53}\right)^2 + \left(\frac{0 \cdot \pi}{9.5}\right)^2 + \left(\frac{1 \cdot \pi}{9.68}\right)^2}} \quad (2)$$

$$= 10.83 \text{ [m]}$$

$$f_{01} = f_{02} = \frac{c}{\lambda_{01}^{TE_{101}}} = \frac{3 \cdot 10^8}{10.83} = 27.7 \text{ [MHz]} \quad (3)$$

Concerning the case c), in cylindrical resonator the first dominant mode is TE_{111} . The resonant frequency can be calculated as follows:

$$\lambda_{03}^{TE_{111}} = \frac{2\pi}{\sqrt{\left(\frac{\alpha'_{11}}{r}\right)^2 + \left(\frac{\pi}{l}\right)^2}}$$

$$= \frac{2\pi}{\sqrt{\left(\frac{1.84}{3.27}\right)^2 + \left(\frac{\pi}{9.68}\right)^2}} = 9.66 \text{ [m]} \quad (4)$$

$$f_{03} = \frac{c}{\lambda_{01}^{TE_{111}}} = \frac{3 \cdot 10^8}{9.66} = 31.05 \text{ [MHz]} \quad (5)$$

The symbols used in equations (2) to (5) are as follows:

λ – wavelength [m],

i, j, k – wave indexes,

a – width of the chamber [m],

b – height of the chamber [m],

c – length of the chamber (cuboidal shape) [m],

l – length of the chamber (cylindrical shape) [m],

r – cylinder radius (cylindrical resonator) [m],

$\alpha'_{11} - 1^{\text{st}}$ derivation of appropriate Bessel's equation root.

According to the above mentioned calculations, the dominant resonance frequency of the chamber would occur between approximately 27 and 31.05 MHz. Based on this expectation, frequencies between 10 and 80 MHz were applied in the framework of the experiment.

3.4 Measurement


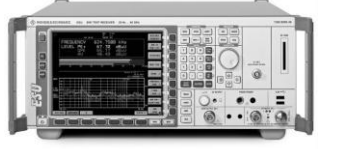
The transmitting antenna was fed with a constant power of 1 mW from a signal generator that was operating in a sweep mode. The transmitting frequency was periodically changed from 10 to 80

MHz with steps of 0.04 MHz. With the dwell time of 0.3 s this determined the measurement time to be 525 s per one measurement point. The frequency spectrum was scanned with Rohde & Schwarz spectrum analyzer ECU that was operated together with the data gathering software EMC32. The spectrum was scanned periodically with a period of 0.1 s, using the bandwidth of 120 kHz. With these settings at least two measurements were made for each frequency transmitted by the omnidirectional antenna. The resolution of the spectral analyzer, regarding to the scanning speed, was set to 625 points, resulting in a virtual frequency step of 112.179 kHz. For each point of measurement (see Fig. 4) the maximum measured values were recorded. After 525 seconds, spectrum of the electrical field for frequencies between 10 and 80 MHz was obtained for the pertinent measurement point, the field probe was moved to another measurement point and the measurements were repeated.

As stated above, the measurement was performed by anisotropic spherical probe HZ-11 [5], which is not sensitive to the orientation of the field. On the other hand, its antenna factor is quite poor, as depicted in Fig. 5. The corrections that were set for the probe and for the cables resulted in a noticeable increase in noise levels. Because there was no need to evaluate the absolute values of the electric field levels, but only differences among the points were recorded, the bias of the measured levels (y-axis drift in the diagrams) was not calibrated and the noise level was considered to be satisfactory.

Settings of the instruments are shown in Table 2.

Table 2. Instruments settings

Generator	
Frequency range	10.0 to 80.0 MHz
Frequency step	0.04 MHz
Dwell time	0.3 s
Output power	0 dBm
Receiver	
Operation mode	Spectral analyser, Computer controlled, Repeated measurement,

	MaxValue Hold
Frequency range	10.0 to 80.0 MHz
Res. bandwidth	120 kHz
Virtual bandwidth	112.18 kHz (625 points in spectrum)
Scanning time	0.1 s
Antenna factor correction	E-Field probe R&S HZ11 (See fig. 7)

TE011	29.13 MHz
TE111	37.13 MHz
TE102	38.71 MHz
TE201	48.20 MHz
TE212	54.40 MHz
TE202	55.40 MHz
TE122	63.60 MHz
Etc.	

Once the data were obtained, their analysis was made in MS Excel in order to visualize remarkable phenomena to be studied.

From the measured responses, the dominant frequency at each of the measured points was identified, as listed in Table IV. The displacement of the dominant frequencies is shown in Fig. 8.

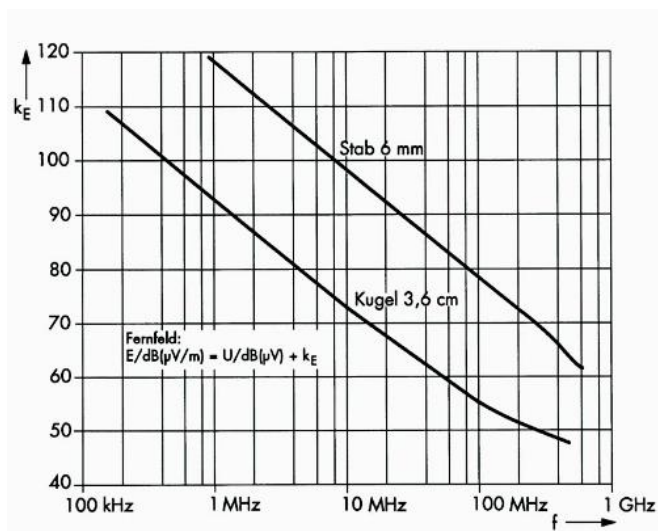


Fig. 7 E-field probe antenna factor (lower curve) [5]

Table 4. Dominant frequencies identified by the measurement

Point of measurement	Frequency [MHz]	Closest mode	Deviation from the calculated frequency [MHz]
A	36.81	TE111	- 0.34
B	36.81	TE111	- 0.34
C	37.15	TE111	+ 0.02
D	28.17	TE101	+ 0.47
E	25.71	TE101	- 1.99
F	35.58	TE111	- 1.55
G	27.95	TE101	+ 0.25
H	27.61	TE101	- 0.09
I	41.41	TE102	+ 2.70
J	50.83	TE201	+ 2.63
K	38.72	TE102	+ 0.01
L	36.03	TE111	- 1.10
M	35.46	TE111	- 1.67
N	38.27	TE102	- 0.44
O	24.25	TE101	- 3.45

4 Results

For each of the points (A) to (O), a frequency response was obtained by the measurement. Consisting of 625 points, the frequency resolution was approximately 112 kHz. A discussion on the results is provided in the chapter below.

4.1 Resonant modes

On the basis of the initial experiments it was found that the measured chamber tended to act as a cuboidal resonator with the first dominant frequency of approximately 27.7 MHz. Consequently, higher resonant modes were calculated. These modes are enlisted in Table 3.

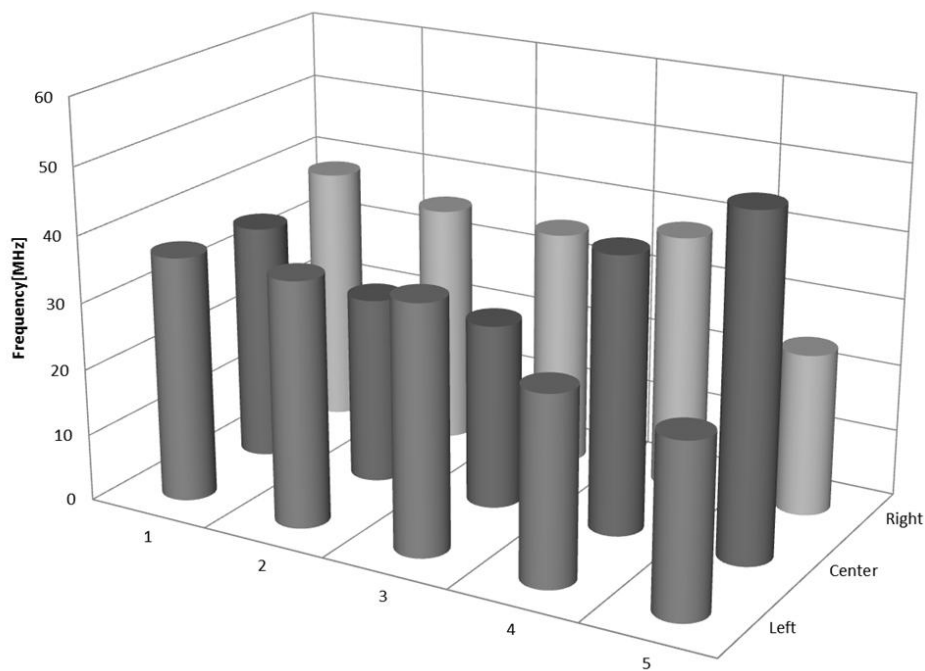
Table 3. Resonant modes of cuboidal resonator

Mode	Frequency
TE101	27.70 MHz

4.2 Maximum intensities

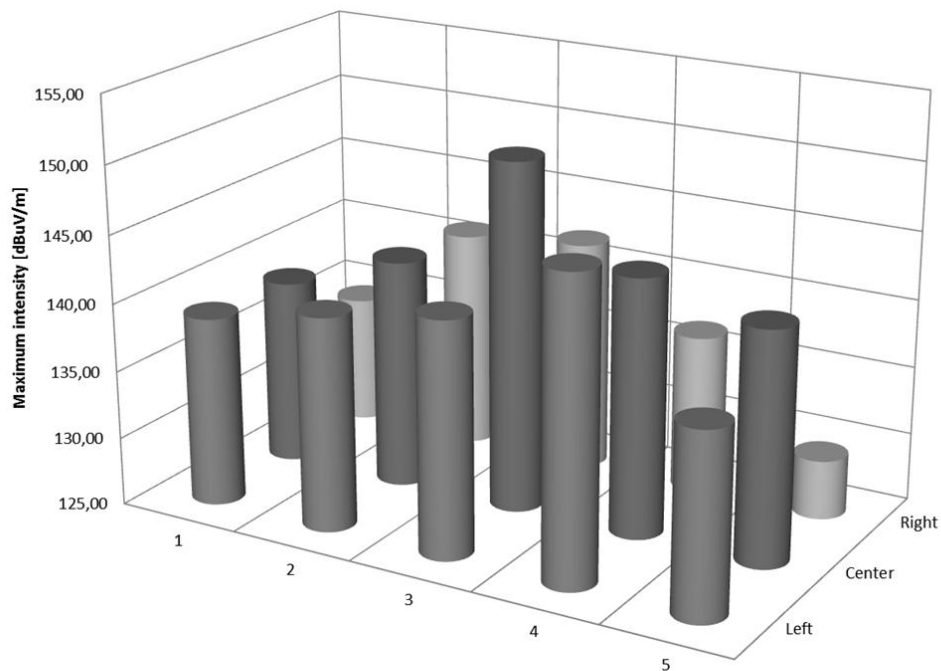
A diagram displaying maximum intensities measured at particular points is shown in Fig. 9. The frequencies of maxima correspond to Table 4. Average intensities are depicted in Fig. 10.

In Fig. 12 there is a set of graphs displaying the electrical field intensity displacement inside the chamber according to the maximums listed in Table 4. Although the grid of measurement points is quite rough, several modes as TE101 or TE102 can be observed.



	1	2	3	4	5
■ Left	36,810897	36,810897	37,147436	28,173077	25,705128
■ Center	35,576923	27,948718	27,612179	41,410256	50,833333
■ Right	38,717949	36,025641	35,464744	38,269231	24,246795

Fig. 8 Displacement of dominant frequencies



	1	2	3	4	5
■ Left	1,39E+02	1,41E+02	1,42E+02	1,47E+02	1,39E+02
■ Center	1,39E+02	1,42E+02	1,51E+02	1,44E+02	1,42E+02
■ Right	1,34E+02	1,41E+02	1,42E+02	1,37E+02	1,29E+02

Fig. 9 Maximum intensities measured at particular points

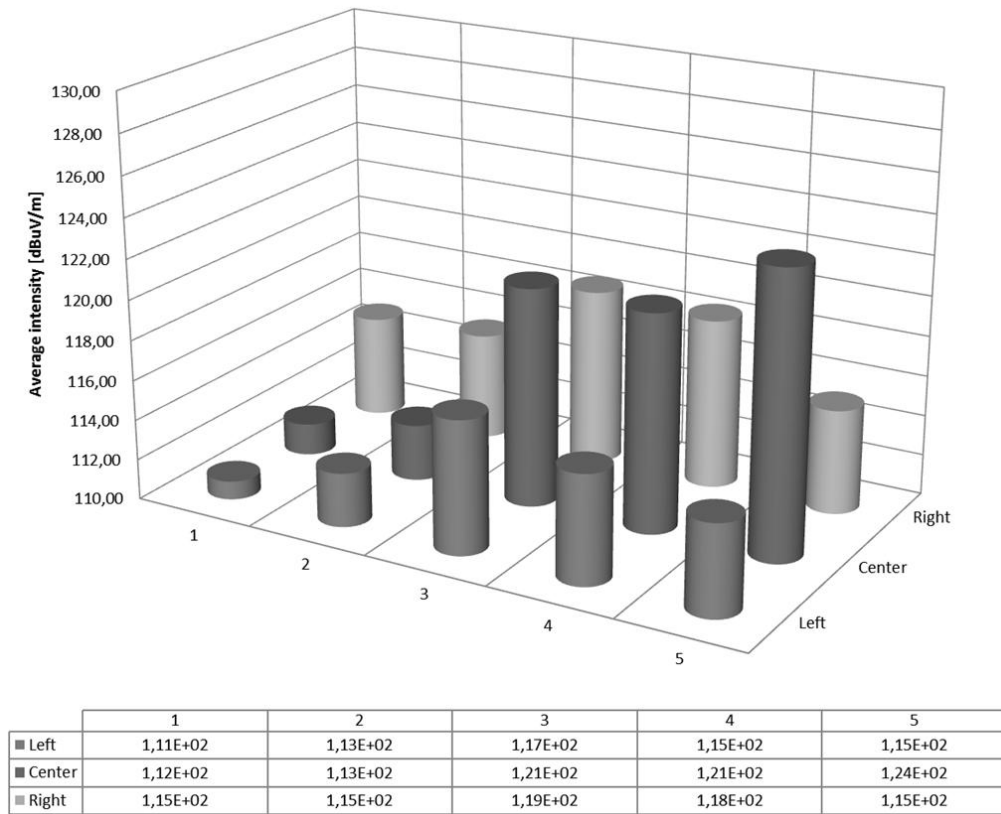


Fig. 10 Intensities at particular points averaged over all measured frequencies

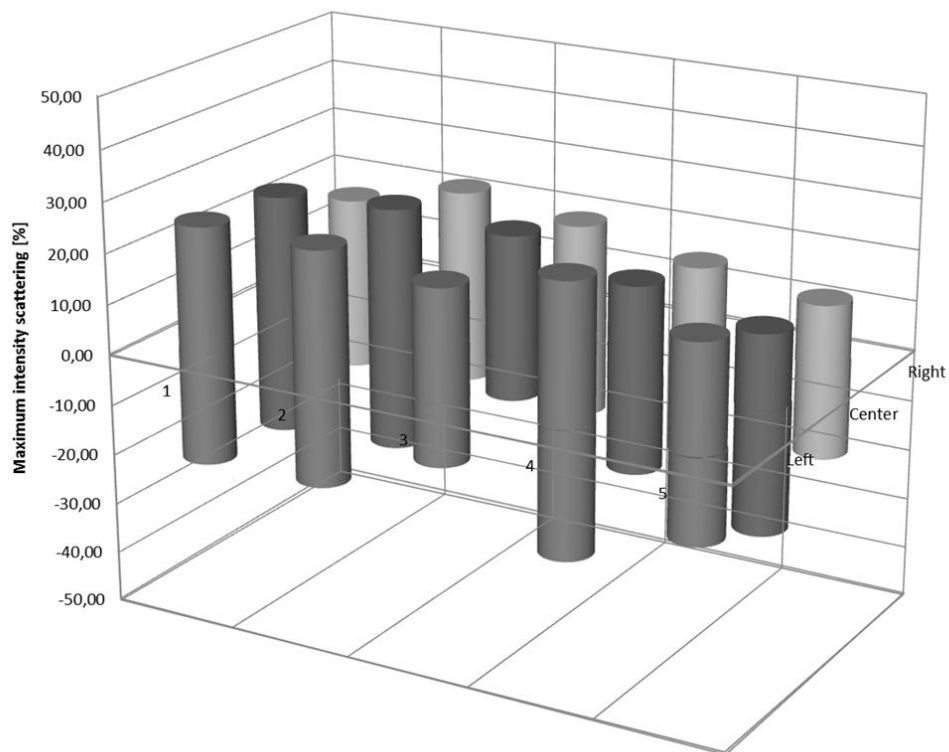


Fig. 11 Scattering rates (positive and negative) of each of the measurement point

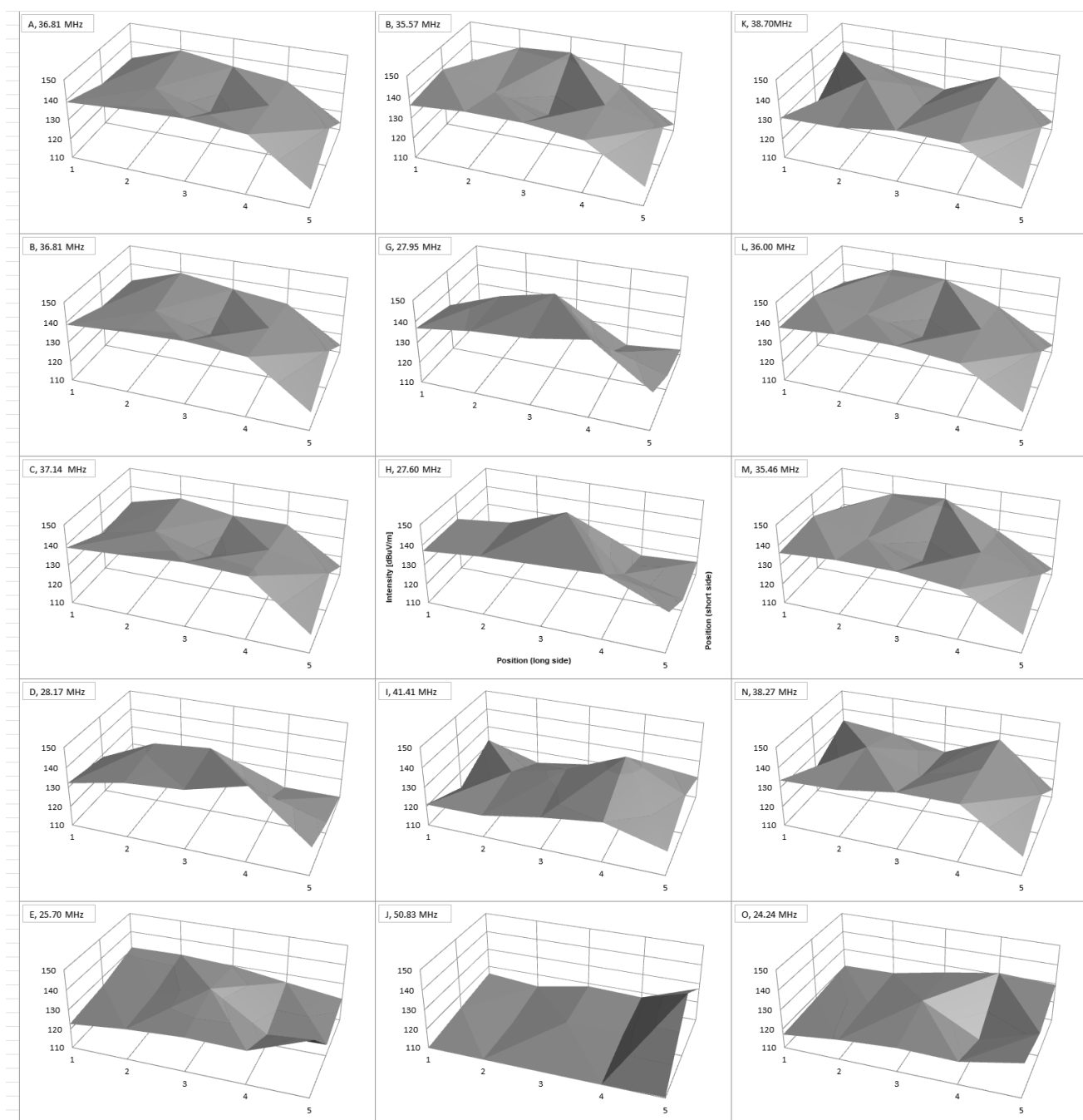


Fig. 12 Electrical field intensity displacement inside the chamber according to the maximums listed in Table IV; the interpretations of all axes are the same as in Fig. 8 to 11.

4.3 Scattering of measured intensities

Provided the field in the chamber was driven with a constant power, not dependent on the frequency, if there was a constant response of the chamber, the intensity of the measured field would be frequency independent. However, according to the measured data, the frequency response was different for each of the measurement points. This phenomenon is described by graphs as shown in Fig. 13 to 17.

The amount of scattering can be interpreted as an indicator of the quality of damping of the room.

Therefore, out of 625 measured frequency points for each point of measurement, the maximum and the minimum intensity were found and the rate of scattering was calculated according to equations (6) and (7).

As mentioned above, providing the measurements were taken for 625 frequencies at each point, obtaining values V_1 to V_{625} , positive scattering ratio for each point can be defined as follows:

$$S^+ = \frac{\max\{V_i\}_{i=1}^{625} - \frac{\sum_{i=1}^{625} V_i}{625}}{\frac{\sum_{i=1}^{625} V_i}{625}} \cdot 100 [\%] \quad (6)$$

In the same way, negative scattering ratio can be defined as follows:

$$S^- = \frac{\min\{V_i\}_{i=1}^{625} - \frac{\sum_{i=1}^{625} V_i}{625}}{\frac{\sum_{i=1}^{625} V_i}{625}} \cdot 100 [\%] \quad (7)$$

Both equations (6) and (7) provide the information on the extreme deviation from the average value. For better comprehension, the scattering values are listed in Table 5.

Table 5. Relative intensity scattering (frequency-dependent deviation)

Point of measurement	Positive scattering [%]	Negative scattering [%]	Total scattering [%]
A	25.25	-22.11	47.36
B	24.89	-21.53	46.42
C	22.00	-12.30	34.50
D	27.58	-25.06	52.64
E	20.93	-16.59	37.52
F	24.26	-23.82	48.08
G	25.74	-22.47	48.21
H	24.61	-7.86	32.47
I	19.15	-17.49	36.64
J	14.54	-24.26	38.80
K	16.84	-18.55	35.39
L	22.32	-16.85	39.17
M	19.55	-19.29	38.84
N	15.39	-17.81	33.20
O	12.29	-18.30	30.59

The figures depicted below provide another view of the frequency response of the chamber in dependence on the placing of measurement.

4.3.1 Longitudinal cuts

The diagrams depicted in Fig. 13 to Fig. 15 are related to longitudinal cuts, displaying how the intensity of the electrical field depends on frequency and position.

Each diagram consists of five measurements that were obtained in a longitudinal plane inside the chamber. The planes are, according to Fig. 4, defined by sets of points (A) to (E), (F) to (J) and (K) to (O).

According to Fig. 13, Fig. 14 and Fig. 15 it is obvious, that there are increased levels of intensity at frequencies between 20 and 40 MHz, being probably related to the dominant modes. It is interesting that the frequencies at which there are maximum electrical field intensities are dependent on the position inside the chamber.

4.3.2 Transversal cuts

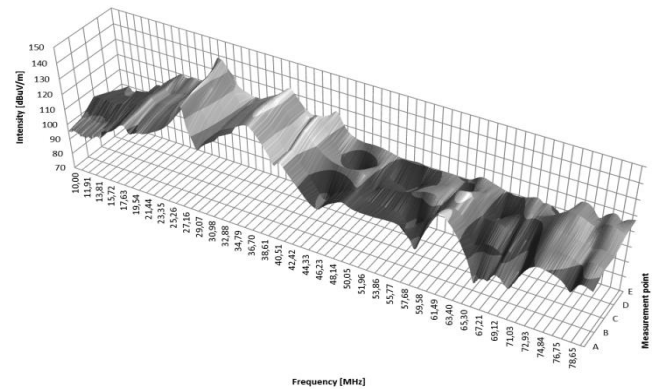


Fig. 13 Dependence of intensity on frequency and position (left part of the chamber)

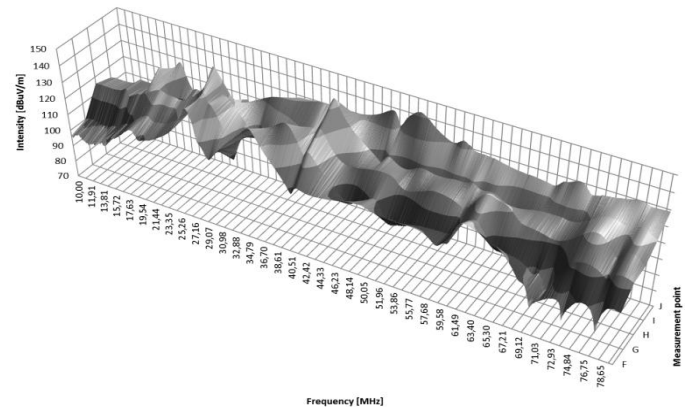


Fig. 14 Dependence of intensity on frequency and position (central part of the chamber)

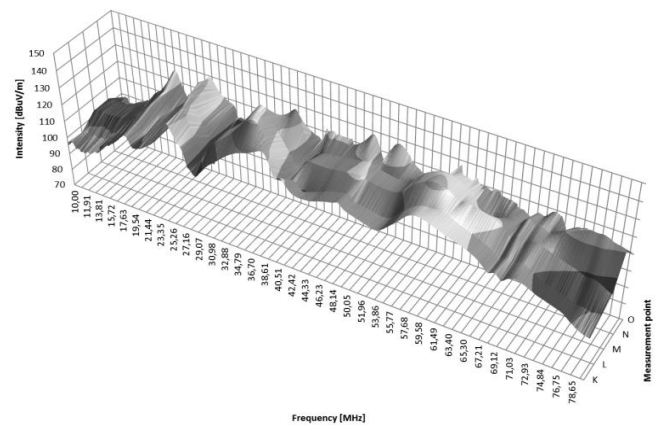


Fig. 15 Dependence of intensity on frequency and position (right part of the chamber)

From the gathered data, five transversal planes can be considered (AFK, BGL, ..., EJO). The values of all three points in each plane were averaged and all five averages were visualized in a 3D chart, showing the dependency of electrical field intensity on frequency and location (transversal plane). This diagram is shown in Fig. 9.

For each of the transversal planes there were also 2D charts created. All these charts were merged into one in order that the characteristic features could be observed. The merged chart is depicted in Fig. 17. It shows that at almost all points the resonant peaks can be observed in the neighborhood of 25 and 35 MHz. The only exception is observed in the plane EJO that shows very poor resonance in the neighborhood of 35 MHz, but higher intensities around 50 MHz. Generally it can be stated that the increase of intensity at the resonant frequencies is up to 20 dB compared to the average, which is quite a considerable value.

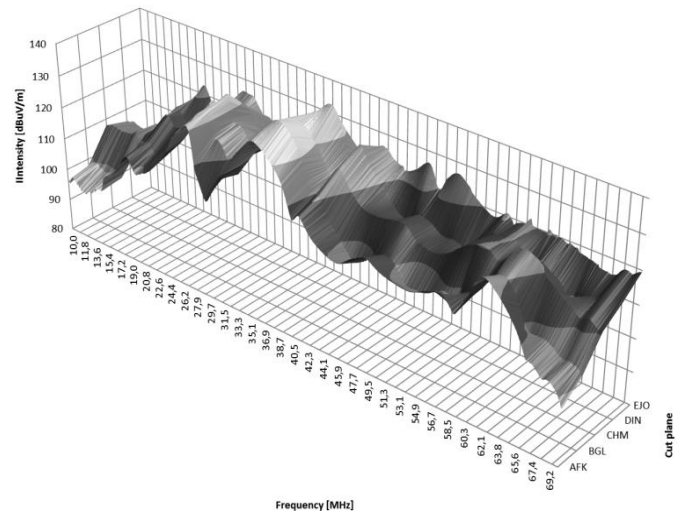


Fig. 16 Dependence of intensity on frequency and location (averages through transversal cuts)

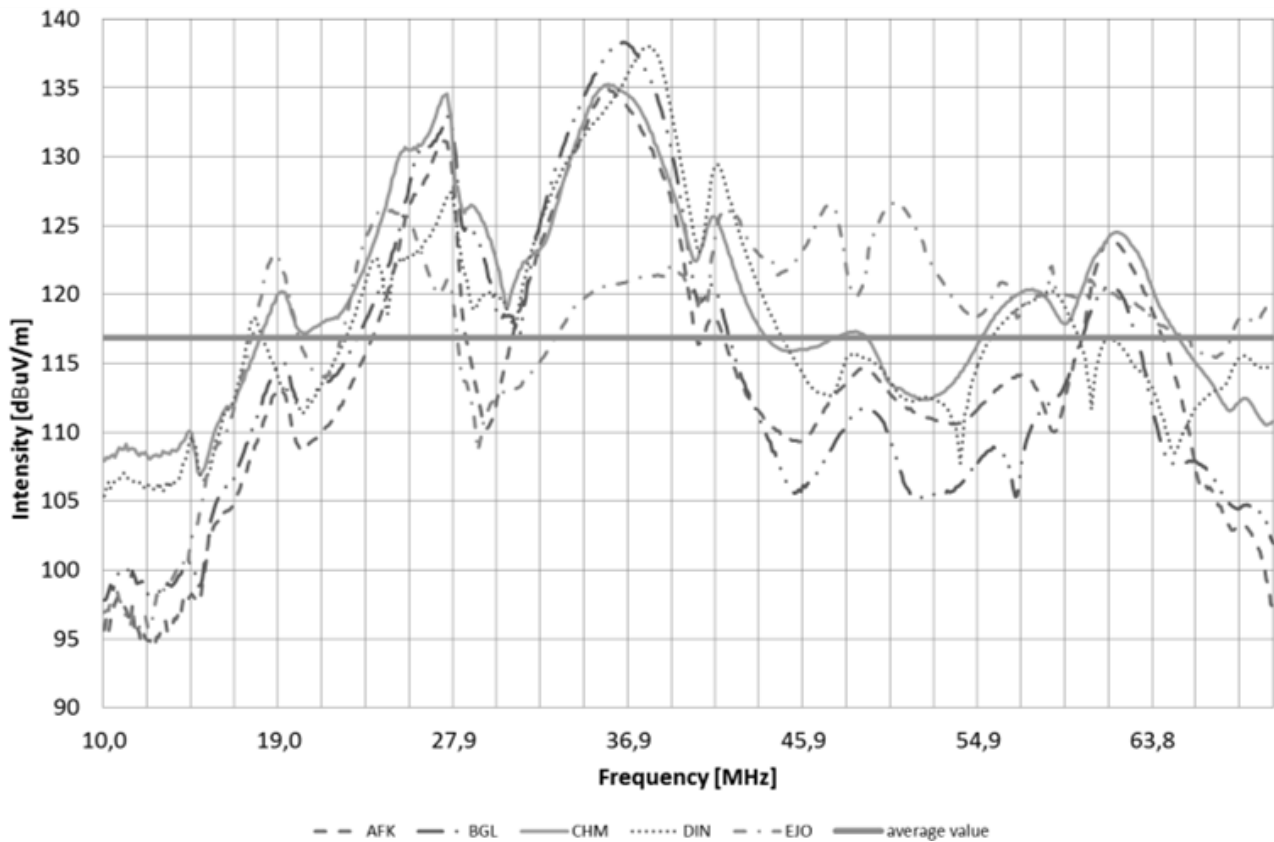


Fig. 17 2D expression of Fig. 16

5 Discussion

The results obtained by the measurement were analyzed in different ways. Although the results at some points seem to be difficult to interpret and a larger quantity of accuracy increasing measurements seems to be necessary, several conclusions can be made.

Even though the chamber is equipped with two different types of absorbers, the reflections at its frequency low-end are not suppressed perfectly. Several dominant frequencies can be observed, indicating mainly the frequency modes TE101 and TE102 or TE111 respectively. Some of the modes can be observed in Fig. 12.

In Fig. 9 the displacement of maximum intensities within the chamber is depicted, showing that the highest intensity can be observed in the center of the chamber at a frequency of 27.61 MHz, which quite well corresponds to the basic frequency mode TE101 as calculated by equation (3).

However, the effect of damping of the chamber by the absorbers can be observed as well. Although, as stated above, several frequency modes are observable, but it can be stated, that their damping is quite considerable. By applying 3 dB criteria, the quality factor of the resonant element can be calculated as [7]:

$$Q = \frac{f_0}{B_{3dB}} \quad (8)$$

In (8) f_0 means the resonant frequency and B_{3dB} means the bandwidth in which the power decrease in neighborhood of the resonant frequency is equal to 3 dB. According to Fig. 17 and considering the transversal plane through points (C), (H) and (M), for the frequency mode TE101 the central frequency f_0 is 27.61 MHz and the bandwidth B_{3dB} is approximately 2.25 MHz. Therefore the quality factor at this point can be estimated to approximately $Q = 12.27$. According to [3] the cavity resonators with similar dimensions and at similar frequencies reach $Q > 1,000$. With this consideration, $Q = 12.27$ can be accepted as a satisfactory value.

The effect of damping can also be observed from Fig. 13 to Fig. 15. Although the chamber is symmetrical, the frequency responses are different in each of the longitudinal cuts. It also can be observed that the higher frequency modes are damped quite well.

In Fig. 8 the displacement of dominant

frequencies is depicted. As stated in the text above, except for points (I) and (J) the values quite well correspond to the lowest frequency modes that can occur within the space of the chamber. The relevance of the values displayed for points (I) and (J) is quite ambiguous, as these points show also relatively low value of intensity scattering (see Fig. 11 and Table 5). Therefore, for the points (I) and (J) there is a probability that the lowest possible frequency modes are quite well damped and therefore the algorithm searching for highest values identified the higher frequency modes as dominant. On the other hand, this statement can be questioned on the basis of Fig. 10 and Fig. 17. The graph in Fig. 10 indicates that the average intensities measured at points (I) and (J) are rather high. The graph in Fig. 17 shows that in the transversal cut through the points (E), (J) and (O) the frequencies around 40 MHz are damped rather poorly compared to other transversal cuts.

6 Conclusion

This paper deals with the problem of electrical field displacement within a semi anechoic chamber that is on duty in Tomas Bata University in Zlin. Based on the expectations that the semi anechoic chamber tends to behave partly as a damped cavity resonator, the authors made frequency response measurements in 15 points inside the chamber and provided a discussion on the obtained results. The measurements were made by means of an anisotropic electrical field probe, using computer-driven automated instrumentation.

Although the amount of measurement points was quite small, it was shown that the chamber behaves as expected. Minimums and maximums can be observed within the area of the chamber in dependence on frequency and location. This phenomenon is most evident between the calculated dominant mode frequencies and approximately 70 MHz, because below approximately 20 MHz no dominant modes can occur and above 70 MHz the attenuation of the reflections is quite effective due to combinations of flat ferrite and pyramidal absorbers mounted across the walls of the chamber.

As it became clear that the expectations were valid, the authors decided to make new set of measurements with increased number of measurement points in order to increase the explanatory power of the data. Based on more accurate data, the correction methods can be proposed so the measurement of electromagnetic

field radiations by tested equipment could be processed with higher accuracy.

The contribution of the research can be found in several aspects. First of all, it was demonstrated that the semi anechoic chamber still suffers from reflections although it is fully equipped with absorbers according to the manufacturer's documentation. This is acceptable when standardized measurements of various devices are processed according to international standards as the standards are designed in a way to minimize the impact of this phenomenon. On the other hand, the reflections inside the chamber should be taken into consideration at all scientific measurements. Secondly, a good knowledge of the chamber can make the preliminary measurements of equipment interferences easier, because it gives the operator information on probably the best position of the receiving antenna.

Recently, further research on this topic is in progress.

Acknowledgement

This work was supported in part by the European Regional Development Fund under the project CEBIA-Tech No. CZ.1.05/2.1.00/03.0089, and by OPVK project CZ.1.07/2.3.00/30.0035.

References:

- [1] S. Radu., *Engineering Aspect of Electromagnetic Shielding*, Sun Microsystems
- [2] Compliance Engineering, *Flat Ferrite RF Absorber: SFA version* [online]. [cit. 2014-04-07].
- [3] J. Svačina, *Electromagnetic compatibility: Principles and notes* [Elektromagnetická kompatibilita: Principy a poznámky], 1st edition. Brno: Vysoké učení technické, 2001. ISBN 80-214-1873-7.
- [4] Frankonia, *Anechoic Chambers / RF-Shielded Rooms*, 2012
- [5] Rohde & Schwarz: *Probe Set HZ-11 for E and H near-field Measurements*, Probe set description
- [6] Z. Trnka, *Theory of Electrical Engineering* [Teoretická elektrotechnika], SNTL Alfa, Bratislava, 1972, Czechoslovakia
- [7] Radio-Electronics.com: *Quality Factor* [online]. [cit. 2014-09-02]
- [8] T.I Maris et al., *Electromagnetic field identification using artificial neural networks*, In *Proceedings of the 8th WSEAS International Conference on Neural Networks*, Vancouver, British Columbia, Canada, June 19-21, 2007
- [9] M. Mann, B. Gutheil, J. Zastrau, P. Weiss, *Electromagnetic field measurements – Means of verification*, In *Proc. of the 5th WSEAS/IASME Int. Conf. on Electric Power Systems, High Voltages, Electric Machines*, Tenerife, Spain, December 16-18, 2005 (pp 591-595)
- [10] M. Pospisilik, J. Soldan, *Electromagnetic field distribution within a semi anechoic chamber*, In *Proceedings of the 18th International conference on systems*, Santorini island, Greece, July 17-21, 2014, ISBN 978-1-61804-244-6
- [11] S. Staines A., Neri F. A *Matrix Transition Oriented Net for Modeling Distributed Complex Computer and Communication Systems*. *WSEAS Transactions on Systems*, 13, WSEAS Press (Athens, Greece), pp. 12-22, 2014
- [12] Camilleri M., Neri F., Papoutsidakis M. An Algorithmic Approach to Parameter Selection in Machine Learning using Meta-Optimization Techniques. *WSEAS Transactions on Systems*, 13, WSEAS Press (Athens, Greece), pp. 202-213, 2014
- [13] M. Papoutsidakis, D. Piromalis, F. Neri, M. Camilleri (2014). *Intelligent Algorithms Based on Data Processing for Modular Robotic Vehicles Control*. *WSEAS Transactions on Systems*, 13, WSEAS Press (Athens, Greece), pp. 242-251, 2014
- [14] M. Pospisilik, M. Adamek. *Logarithmic VU Meter Driver*, In VASEK, V. et al. *Proceedings of the 13th WSEAS International Conference on Automatic Control, Modelling & Simulation*, 1. Vyd., Lanzarote: WSEAS Press, 2011, Recent Researches in Automatic Control, s. 331 – 336. ISBN 978-1-61804-004-6
- [15] M. Pospisilik, M. Adamek. *Advanced Voltage Controlled Amplifier for Volume Expanders*, In VASEK, V. et al. *Proceedings of the 13th WSEAS International Conference on Automatic Control, Modelling & Simulation*, 1. Vyd., Lanzarote: WSEAS Press, 2011, Recent Researches in Automatic Control, s. 325 – 330. ISBN 978-1-61804-004-6
- [16] Pekař, L., Neri, F. An introduction to the special issue on time delay systems: Modelling, identification, stability, kontrol and applications, *WSEAS Transactions on Systems*, 11 (10), pp. 539-540, 2012